INTERNATIONAL JOURNAL OF QUANTUM CHEMISTRY SYMP. NO. 10, 383-403 (1976)

Combined Fourier Transform and Discrete Variational Method Approach to the Self-Consistent Solution of the Electronic Band Structure Problem within the Local Density Formalism

A. ZUNGER AND A. J. FREEMAN

Department of Physics and Materials Research Center, Northwestern University, Evanston, Illinois 60201

Abstract

This novel approach combines a discrete variational treatment of all potential terms arising from the superposition of the spherical overlapping atomic charge densities with a rapidly convergent Fourier series representation of all multicenter nonspherical potential terms. The basis set consists of the exact numerical atomic valence orbitals, augmented by charge transfer states, virtual atomic states, and single analytic Slater orbitals for increased variational flexibility. The initial potential is a non-muffin-tin overlapping atomic potential including nongradient local density exchange and correlation terms. Full self-consistency is obtained by a procedure that combines an iterative scheme within the superposition model with a self-consistent optimization of the Fourier components of the nonspherical charge density terms. Ground-state properties such as structure factors and cohesive energy are computed. The results for diamond show very good agreement with experiment. Comparison of the results with the Hartree–Fock calculation is discussed.

1. Introduction

It is now widely recognized that energy band theory has become a powerful and sophisticated method for studying a wide spectrum of solid-state properties. The proliferation of energy band schemes and their application to increasingly diverse problems attests to the current popularity of band theory. Increasingly too, however, its very success in describing a host of sophisticated new solid-state experiments has led to a "tide of rising expectations" which the various existing computational energy band schemes (such as APW, OPW, KKR, etc.) have been hard pressed to satisfy. In addition to challenging experiments performed on important materials having complex crystallographic structures, these new experiments have demanded not only theoretical descriptions of high-resolution eigenvalue phenomena, but also detailed and precise solid-state wave functions with which to determine the expectation values of different observable operators. Such a demanding test of the predictions of one-electron theory has the additional virtue in permitting, by their comparison with experiment, accurate determinations of the relative magnitude and importance of many-body effects in real solids.

In this paper we describe a new approach to the fully self-consistent solution of the one-particle equations in a periodic solid within the local density functional formalism [1]. It is specifically designed and developed to incorporate special features with which to overcome difficulties encountered by other methods. Specifically, as will be shown

in detail, the method combines a discrete variational treatment of all potential terms (Coulomb, exchange, and correlation) arising from the superposition of spherical atomic-like overlapping charge densities, with a rapidly convergent three-dimensional Fourier-series representation of all the multicenter potential terms that are not expressible by a superposition model. The *basis set* consists of the exact numerical valence orbitals obtained from a direct solution of the local-density atomic one-particle equations. To obtain increased variational freedom, this basis set is then augmented by virtual (numerical) atomic orbitals, charge-transfer (ion-pair) orbitals, and "free" Slater one-site functions. The *initial crystal potential* consists of a non-muffin-tin atomic superposition potential, including nongradient free-electron correlation terms calculated beyond the random-phase-approximation. The *Hamiltonian matrix elements* between Bloch states are calculated by the three-dimensional Diophantine integration scheme of Painter and Ellis [2], thereby avoiding the usual multicenter integrations encountered in the LCAO tight-binding formalism. *Self-consistency* is obtained in two states; in the first stage (charge and configuration self-consistency), the atomic superposition potential and the corresponding numerical basis orbitals are modified simultaneously and nonlinearly by varying (iteratively) the atomic occupation numbers (on the basis of the computed Brillouin-zone averaged band population) so as to minimize the deviation $\Delta\rho(\mathbf{r})$ between the band charge density and the superposition charge density. This step produces the "best" atomic configuration (for the employed numerical basis orbitals) within the superposition model for the crystal charge density and tends to remove all the sharp "localized" features in the function $\Delta\rho(\mathbf{r})$ by allowing for intraatomic charge redistribution to take place. Having obtained a low-amplitude smooth function $\Delta\rho(\mathbf{r})$ that contains zero charge, we proceed in the second stage of self-consistency to solve the three-dimensional multicenter Poisson equation associated with $\Delta\rho(\mathbf{r})$ through a Fourier series representation of $\Delta\rho(\mathbf{r})$. The solution of the band problem is repeated until the changes in the Fourier coefficients of $\Delta\rho(\mathbf{r})$ in successive interactions are lower than a prescribed tolerance. The *calculated observables* include the total crystal ground-state energy, equilibrium lattice constants, electronic pressure, X-ray scattering form factors, nuclear contact densities, momentum density, one-electron band structure, and interband oscillator strength.

2. Scope and Definition of the Problem

The method we describe here is designed to solve effective one-particle equations using a simplified form for the exchange and correlation functional for interacting electron systems due to Hohenberg and Kohn [1] and a general LCAO expansion in a self-consistent non-muffin-tin scheme. The method has a different starting point from that characterizing the Hartree–Fock scheme as applied to solids [3, 4] in that it relies on replacing the usual Hartree–Fock exchange operator by the first few terms in the expansion of the functional derivative of the total exchange and correlation energy of an interacting electron system [1]. Carrying out a fully self-consistent calculation on real solids within this approach would thus provide a way of comparing the predictions of the local density functional (LDF) formalism both with previous Hartree–Fock calculations and with experiment. Since the basic effective one-particle equations in the LDF formalism have been extensively discussed by Hohenberg and Kohn [1], Kohn and Sham [5], and others, we will only briefly state the main results and define and equations to be solved.

The general Hohenberg–Kohn theorem states that the ground-state wave function, and hence all ground-state properties of an interacting electron system, are functionals of the electron density $\rho(\mathbf{r})$ and that in the presence of an external potential $v_{\text{ext}}(\mathbf{r})$ the ground-state total energy can be written as

$$E[\rho(\mathbf{r})] = \int v_{\text{ext}}(\mathbf{r})\rho(\mathbf{r})d\mathbf{r} + G[\rho(\mathbf{r})] \tag{1}$$

where $G[\rho(\mathbf{r})]$ is a universal functional of $\rho(\mathbf{r})$ and is independent of the external potential $v_{\text{ext}}(\mathbf{r})$. Identifying $v_{\text{ext}}(\mathbf{r})$ (for a polyatomic system) as the nuclear–nuclear Coulomb potential plus the electron–nuclear potential, the total energy can be written (aside from the constant nuclear–nuclear term) as

$$E[\rho(\mathbf{r})] = \int \rho(\mathbf{r}) \left[\sum_m \frac{Z_m}{|\mathbf{r} - \mathbf{R}_m|} + \frac{1}{2} \int \frac{\rho(\mathbf{r}')}{|\mathbf{r} - \mathbf{r}'|} d\mathbf{r}' \right] d\mathbf{r} + T_s[\rho(\mathbf{r})] + E_{\text{xc}}[\rho(\mathbf{r})] \tag{2}$$

where Z_m denotes the nuclear charge of the particle at site $\mathbf{R}_m$, $T_s[\rho(\mathbf{r})]$ denotes the kinetic energy of the noninteracting electron system, and $E_{\text{xc}}[\rho(\mathbf{r})]$ denotes the total exchange and correlation energy of the interacting inhomogeneous electron system. Applying a variation with respect to $\rho(\mathbf{r})$ and replacing the functional derivative of $T_s[\rho(\mathbf{r})]$ with respect to the density $\rho(\mathbf{r})$ by the exact kinetic energy operator, one obtains the one-particle equation

$$\left\{ -\frac{1}{2}\nabla^2 + \left[\sum_m \frac{Z_m}{|\mathbf{r} - \mathbf{R}_m|} + \int \frac{\rho(\mathbf{r}')}{|\mathbf{r} - \mathbf{r}'|} d\mathbf{r}' \right] + \frac{\delta E_{\text{xc}}[\rho(\mathbf{r})]}{\delta \rho(\mathbf{r})} \right\} \psi_j(\mathbf{r}) = \epsilon_j \psi_j(\mathbf{r}) \tag{3}$$

where $\rho(\mathbf{r})$ is related to the eigenfunctions $\psi_j(\mathbf{r})$ of the first σ_{oc} occupied levels in the ground state by

$$\rho(\mathbf{r}) = \sum_{j=1}^{\sigma_{\text{oc}}} \psi_j^*(\mathbf{r})\psi_j(\mathbf{r}) \tag{4}$$

The key problem in using Equation (3) is, of course, the lack of a knowledge of $E_{\text{xc}}[\rho(\mathbf{r})]$ and its functional derivative. $E_{\text{xc}}[\rho(\mathbf{r})]$ can be expanded in the well-known gradient series [5–8] as

$$E_{\text{xc}}[\rho(\mathbf{r})] = \int \rho(\mathbf{r})(\epsilon_x[\rho(\mathbf{r})] + \epsilon_c[\rho(\mathbf{r})] + C_s[\rho(\mathbf{r})]\rho^{-7/3}(\mathbf{r})(\nabla\rho(\mathbf{r}))^2 + \cdots)d\mathbf{r} \tag{5}$$

where $\epsilon_x[\rho(\mathbf{r})]$ and $\epsilon_c[\rho(\mathbf{r})]$ are exchange and correlation energies per electron of a uniform electron gas with local density $\rho(\mathbf{r})$, and $C_s[\rho(\mathbf{r})]$ is the first gradient coefficient given by Rasolt and Geldart [6]. Retaining only nongradient terms in Equation (5) yields for the functional derivative of $E_{\text{xc}}[\rho(\mathbf{r})]$ the exchange and correlation parts of the chemical potential $F_{\text{ex}}[\rho(\mathbf{r})]$ and $F_{\text{corr}}[\rho(\mathbf{r})]$, respectively,

$$\frac{\delta E_{\text{xc}}[\rho(\mathbf{r})]}{\delta \rho(\mathbf{r})} \cong F_{\text{ex}}[\rho(\mathbf{r})] + F_{\text{corr}}[\rho(\mathbf{r})] \tag{6}$$

where

$$F_{\text{ex}}[\rho(\mathbf{r})] = \frac{4}{3}\epsilon_x[\rho(\mathbf{r})] = -\left(\frac{3}{\pi}\rho(\mathbf{r})\right)^{1/3} \tag{7}$$

Several attempts have been made to calculate $F_{\text{corr}}[\rho(\mathbf{r})]$ by widely different methods. The agreement between the various estimates is usually to within 10^{-3}–10^{-2} Ryd in the range of metallic densities ([7] and references therein). We have adopted the results of

Singwi and coworkers [8] for $F_{\text{corr}}[\rho(\mathbf{r})]$ as fitted numerically to the analytical form [7]:

$$F_{\text{corr}}[\rho(\mathbf{r})] = -\frac{B}{\pi\alpha A}\ln(1 + X^{-1}) \tag{8}$$

where $X = r_s(\mathbf{r})/A$; $(4\pi/3)\, r_s^3(\mathbf{r}) = \rho(\mathbf{r})^{-1}$, and $A = 21$, $C = 0.045$, $B = 0.7734$, and $\alpha = 0.52106$ are numerical constants. Equation (3) with the functionals of the type given in Equations (6)–(8) have been previously solved for atoms [9] and some molecules [10] (in a spin-polarized scheme), yielding very good results for charge densities and total ground-state energies. The total ground-state electronic energy is given by

$$E = \text{KE} + \int \rho(\mathbf{r}) \left[\sum_m \frac{Z_m}{|\mathbf{r} - \mathbf{R}_m|} + \frac{1}{2}\frac{\rho(\mathbf{r}')}{|\mathbf{r} - \mathbf{r}'|}\, d\mathbf{r}' \right] d\mathbf{r} + \int \rho(\mathbf{r})[\epsilon_x[\rho(\mathbf{r})] + \epsilon_c[\rho(\mathbf{r})]]\, d\mathbf{r} \tag{9}$$

where KE is the kinetic energy and

$$\epsilon_x[\rho(\mathbf{r})] = -\frac{3}{4}\left(\frac{3}{\pi}\rho(\mathbf{r})\right)^{1/3} \tag{10}$$

The results of Singwi and coworkers [8] for the electron gas correlation energy, as fitted to an analytic form [7], yield

$$\epsilon_c[\rho(\mathbf{r})] = -C\{(1 + X^3)\ln(1 + X^{-1}) + X/2 - X^2 - 1/3\} \tag{11}$$

In this paper we describe a method for solving Equation (3) with the forms of Equations (6)–(8) for periodic solids. The solution would be repeated both for a pure exchange functional ($F_{\text{corr}}[\rho(\mathbf{r})] \equiv 0$) and for $F_{\text{ex}}[\rho(\mathbf{r})] + F_{\text{corr}}[\rho(\mathbf{r})]$ to faciliate comparisons with other calculations. The method is completely general in that it enables treatment of general solids with no restriction on the form of the potential.

In what follows we will discuss the proposed method in terms of (*1*) the basis functions used to expand $\psi_j(\mathbf{r})$, (*2*) the construction of the potential, (*3*) the approach used to compute the Hamiltonian elements, and (*4*) the method for obtaining self-consistency in the solution. We will finally discuss some of the results obtained with the method to date on diamond. Further applications to solid neon, LiF, boron nitride, and TiS_2 are underway.

3. Method

A. Basis Functions

The basis functions used in our scheme can be conveniently classified into four types.

(*a*) *Self-consistent numerical–local orbitals* (NLO) *for the occupied states in the atoms.* These are calculated by direct numerical integration of the central-field one-particle equations for each atom α (in atomic units):

$$\left[-\frac{1}{2}\nabla^2 + g_\alpha(\mathbf{r})\right] \chi^\alpha_{n,l}(\mathbf{r}, \{f^\alpha_{n'l'}, Q^\alpha\}) = \epsilon_{n,l}\chi^\alpha_{n,l}(\mathbf{r}, \{f^\alpha_{n'l'}, Q^\alpha\}) \tag{12}$$

Here $\epsilon_{n,l}$ denotes the atomic-like eigenvalues, and $\chi^\alpha_{n,l}(\mathbf{r}, \{f^\alpha_{n'l'}, Q^\alpha\})$ are the NLO that depend parametrically on the assumed population numbers $f^\alpha_{n'l'}$ of all N_{oc} occupied

one-electron levels $n'l'$ and on the net ionic charge Q^α of site α. The ionic charge Q^α is simply related to the nuclear charge Z^α by

$$Q^\alpha = Z^\alpha - \sum_{n,l}^{N_{oc}} f_{n,l}^\alpha \tag{13}$$

The potential $g_\alpha(\mathbf{r})$ for site α is taken in the local density formalism as

$$g_\alpha(\mathbf{r}) = v_{co}^\alpha(\mathbf{r}) + v_{ex}^\alpha(\mathbf{r}) + v_{corr}^\alpha(\mathbf{r}) + A^\alpha(\mathbf{r}) \tag{14}$$

where $v_{co}(\mathbf{r})$, $v_{ex}(\mathbf{r})$, and $v_{corr}(\mathbf{r})$ are the Coulomb, exchange, and correlation potentials, respectively, derived from the total ground-state electronic charge density of the αth atom:

$$\rho^\alpha(\mathbf{r}) = \sum_{n,l}^{N_{oc}} f_{n,l}^\alpha [\chi_{n,l}^\alpha(\mathbf{r}, f_{n'l'}^\alpha, Q^\alpha)]^2 \tag{15}$$

through the αth-site Poisson equation and the local exchange and correlation functionals $F_{ex}[\rho^\alpha(\mathbf{r})]$ and $F_{corr}[\rho^\alpha(\mathbf{r})]$ defined in Equations (7) and (8). $A(\mathbf{r})$ is an additional potential term, chosen to tailor the NLO $\{\chi_{n,l}^\alpha(\mathbf{r})\}$ for their use in a variational calculation in the solid. One may thus generate through Equation (12) atomic basis functions that are less diffuse than regular atomic orbitals by taking $A(\mathbf{r})$ as a Latter tail correction [11], a square-well potential [12], or by adopting an Adams–Gilbert localizing term [13] $A(\mathbf{r})$, modified for local density equations. It is to be noted that the ϵ_{nl} have no direct physical meaning and that Equation (12) is used only to generate basis orbitals that would effectively span the occupied manifold in the polyatomic system.

Equation (12) is solved self-consistently (for a fixed set of population numbers $\{f_{n,l}^\alpha\}$ and ionic charge Q^α) by recomputing the one-site potential $g_\alpha(\mathbf{r})$ on the basis of the density $\rho^\alpha(\mathbf{r})$ found at each iteration stage. The resulting orbitals $\chi_{n,l}^\alpha(\mathbf{r})$ thus depend not only on the population of the n,lth level, but also on all other occupied states. We note that the set $\chi_{n,l}^\alpha(\mathbf{r})$, obtained in a tabular form, is not fitted to any analytical basis (Slater orbitals, Gaussian orbitals, etc.) but instead is used directly in our variational calculation in the solids in order to avoid loss of accuracy and the well-known disadvantages of the usual analytical orbitals in LCAO-type variational calculations on polyatomic systems. This numerical basis set will subsequently be optimized nonlinearly in the crystalline variational calculation by varying the set $\{f_{n,l}^\alpha, Q^\alpha\}$ and repeating the solution of Equation (12) so as to obtain increased variational freedom. The NLOs form a very compact and flexible basis set whose quality, as estimated from molecular calculations [12, 14] and from our present experience, is at least comparable to a double-zeta Slater set.

(*b*) *Numerical virtual one-site orbitals.* These are just the solutions of Equation (12) for the unoccupied levels. It is to be noted that while the occupied NLOs are likely to be efficient in spanning the occupied manifold in periodic systems due to the atomic-like character of the low-lying crystalline states, there is no reason for the virtual solutions to be equally effective.

The extremely diffuse character of the high-energy virtual orbitals [even after some contraction has been obtained by proper choice of $A(\mathbf{r})$ in Equation (12)] makes them both numerically inconvenient (due to the need to perform lattice sums extending to a rather long range) and variationally unimportant (since the long-range character of the crystal states is already efficiently reproduced by the medium-range basis functions in the presence of translational symmetry). In practice we limit our virtual numerical basis set to include only the first two to four virtual levels, up to (and including) the first polarization function. In cases where linear dependence between the Bloch basis functions

is introduced by a virtual state, it is discarded. It should be mentioned that due to the nonlinear optimization of the numeric basis orbitals in our scheme, some of the formerly virtual orbitals become fractionally populated during iterations, and hence their short-range character is recovered.

Basis sets of the type (a) and (b) described form our standard working basis for computing the one-electron eigenvalues in the solid. In further calculations this set is augmented by the following two additional sets.

(*c*) *Numerical charge-transfer (ion-pair) orbitals.* A limited configuration mixing along the lines of valence-bond methodology is obtained by placing on each site several NLO sets, corresponding to different Q^α. [Thus in the diamond calculation to be described, in addition to neutral ($Q^\alpha = 0$) NLOs and virtual functions, we place on each carbon atom two additional NLO sets corresponding to the numerical orbitals of anionic and cationic carbon.] Although the eigenvalue spectra (band structure) are not expected to change much since the $Q^\alpha = 0$ NLO set plus the virtual numeric set are already extremely efficient, many-electron observables, such as the total ground-state energy, might require such an enlarged set.

(*d*) *Free uncontracted Slater orbitals with high nl quantum numbers and medium-range exponents.* These are added to increase variational freedom in the virtual space when the addition of extra virtual numerical orbitals [type (b)] is excluded due to their high diffusivity. We note that due to the complete avoidance of analytical and semi-analytical algorithms for computing the Hamiltonian matrix elements (see below), we are able to treat very general basis functions with no additional computation costs, thus efficiently exploiting the variational efficiency offered by exact numerical orbitals.

B. Initial Crystal Model Potential

The initial crystal potential used for the first iteration in our self-consistent scheme is the usual superposition model of overlapping spherical atomic potential given by superimposing the individual atomic densities $\rho^\alpha(\mathbf{r})$ [Equation (15)]:

$$\rho^{\text{sup}}(\mathbf{r}) = \sum_{\alpha=1}^{h} \sum_{m=1}^{N} \rho^\alpha(\mathbf{r} - \mathbf{R}_m - \mathbf{d}_\alpha) \tag{16}$$

so that $\rho^{\text{sup}}(\mathbf{r})$ transforms like the totally symmetric Γ_1 representation of the space group in question. $\mathbf{R}_m$ for $m = 1, \cdots, N$ labels the mth unit cell position vector and $\mathbf{d}_\alpha$ for $\alpha = 1, \cdots, h$ denotes the relative location of the αth inequivalent site in the unit cell. In Equation (16) and in further equations we will omit, for brevity, the notation $\{f^\alpha_{n,l}, Q^\alpha\}$ for the parametric dependence of the basis set and charge density on the assumed atomic electron configuration.

The Coulomb potential is partitioned into two parts. The short-range Coulomb superposition potential $V^{\text{sup}}_{\text{SRC}}(\mathbf{r})$ is simply related to the superposition charge density $\rho^{\text{sup}}(\mathbf{r})$ by the Poisson equation and is treated as a discrete lattice sum:

$$V^{\text{sup}}_{\text{SRC}}(\mathbf{r}) = \sum_{\alpha=1}^{h} \sum_{m=1}^{N} v^\alpha_{\text{co}}(\mathbf{r} - \mathbf{R}_m - \mathbf{d}_\alpha) \tag{17}$$

where $v^\alpha_{\text{co}}(\mathbf{r})$ denotes all contributions to the atomic Coulomb potential that are found to fulfill the relation $rv^\alpha_{\text{co}}(r) \leqslant 10^{-4}$ for r larger than a threshold value R_t. The lattice sums in Equation (17) are performed up to a maximum range $R_{\text{cut}} \geqslant R_t$ (typically 15–25 a.u.). All the remaining long-range parts in the atomic Coulomb potential are treated as point ions (with charge Q^α) and summed to yield

$$V_{\mathrm{LRC}}^{\mathrm{sup}}(\mathbf{r}) = \sum_{\alpha}^{h} \sum_{m}^{\infty} \frac{Q^{\alpha}}{|\mathbf{r} - \mathbf{R}_m - \mathbf{d}_{\alpha}|} \tag{18}$$

The sum in Equation (18) is performed to convergence by the Ewald method [15].

The exchange model potential $V_{\mathrm{ex}}^{\mathrm{sup}}(\mathbf{r})$ is obtained by applying the local density exchange functional $F_{\mathrm{ex}}[\rho(\mathbf{r})]$ to the superposition charge density $\rho^{\mathrm{sup}}(\mathbf{r})$:

$$V_{\mathrm{ex}}^{\mathrm{sup}}(\mathbf{r}) = F_{\mathrm{ex}}[\rho^{\mathrm{sup}}(\mathbf{r})] = -\left[\frac{3}{\pi} \sum_{\alpha}^{h} \sum_{m}^{N} \rho^{\alpha}(\mathbf{r} - \mathbf{R}_m - \mathbf{d}_{\alpha})\right]^{1/3} \tag{19}$$

The correlation potential $V_{\mathrm{corr}}^{\mathrm{sup}}(\mathbf{r})$ is similarly obtained by applying the correlation local density functional $F_{\mathrm{corr}}[\rho(\mathbf{r})]$ [Equation (8)] to the model charge density

$$V_{\mathrm{corr}}^{\mathrm{sup}}(\mathbf{r}) = F_{\mathrm{corr}}[\rho^{\mathrm{sup}}(\mathbf{r})] \tag{20}$$

It is important to note that due to the nonlinearity of the exchange and correlation functions $F_{\mathrm{ex}}[\rho(\mathbf{r})]$ and $F_{\mathrm{corr}}[\rho(\mathbf{r})]$ (as opposed to the linearity of the Poisson equation), $V_{\mathrm{ex}}^{\mathrm{sup}}(\mathbf{r})$ and $V_{\mathrm{corr}}^{\mathrm{sup}}(\mathbf{r})$ can no longer be represented as a sum of one-center atomic-like terms as is the case for $V_{\mathrm{SRC}}^{\mathrm{sup}}(\mathbf{r})$. Many LCAO techniques, as well as scattered-wave $X\alpha$ methods, are possible only if the potential is representable as a sum of single-site terms, in which case the functionals $F_{\mathrm{ex}}[\rho^{\mathrm{sup}}(\mathbf{r})]$ and $F_{\mathrm{corr}}[\rho^{\mathrm{sup}}(\mathbf{r})]$ are either linearized arbitrarily [16] (for example, $V_{\mathrm{ex}}^{\mathrm{sup}}(\mathbf{r}) \approx \Sigma_m \Sigma_{\alpha} F_{\mathrm{ex}}[\rho^{\alpha}(\mathbf{r} - \mathbf{R}_m - \mathbf{d}_{\alpha})]$ or apportioned into a muffin-tin form [17]. To avoid such extreme approximations, one might also project numerically $F_{\mathrm{ex}}[\rho^{\mathrm{sup}}(\mathbf{r})]$ and $F_{\mathrm{corr}}[\rho^{\mathrm{sup}}(\mathbf{r})]$ onto a single-site fitting basis [18, 19]. Such an approach, aside from involving some loss in accuracy, would require specially designed auxiliary fit functions for each functional appearing in the superposition potential (for example, exchange, correlation) and would tend to become intractable for systems involving a large range of n,l values in the ground-state charge density [19]. Due to the numerical integration algorithm used in our scheme, none of these approximations to the potential are required, and we use the full superposition potential:

$$V^{\mathrm{sup}}(\mathbf{r}) = V_{\mathrm{SRC}}^{\mathrm{sup}}(\mathbf{r}) + V_{\mathrm{LRC}}^{\mathrm{sup}}(\mathbf{r}) + V_{\mathrm{ex}}^{\mathrm{sup}}(\mathbf{r}) + V_{\mathrm{corr}}^{\mathrm{sup}}(\mathbf{r}) \tag{21}$$

in a variational calculation. The superposition potential $V^{\mathrm{sup}}(\mathbf{r})$ is completely defined by specifying the atomic numbers (Z^{α}, $\alpha = 1, \cdots, h$), the assumed space group, and the occupations $\{f_{n,l}^{\alpha}, Q^{\alpha}, \alpha = 1, \cdots, h\}$.

The main shortcomings of the superposition potential in simulating the self-consistent crystal potential (determined from the *crystal* eigenstates) seem to arise from three major limitations.

(*1*) The expansion in Equation (16) involves only one-center terms whose origin is fixed to coincide with existing atomic sites. One would hardly expect the three-dimensional multicenter crystalline potential to be amenable to an accurate projection into such limited single-center sets.

(*2*) The choice of population numbers $\{f_{n,l}^{\alpha}\}$ and ionic-charges Q^{α} that determine the self-consistent atomic charge densities [Equation (15)] to be used in constructing $V^{\mathrm{sup}}(\mathbf{r})$ remains unrelated to the actual population taking place in a crystalline bonding situation.

(*3*) Although $\rho^{\mathrm{sup}}(\mathbf{r})$ transforms like the totally symmetric representation of the space group in question, it is constructed from spherically symmetric site densities $\rho^{\alpha}(\mathbf{r})$, while actual crystal densities might have nonspherical site components that are not describable by an overlapping model such as Equation (16).

In what follows we will treat the multicenter terms that are not amenable to a one-site superposition model [limitation (*1*)] in an exact fashion by supplementing the superposition potential by a Fourier representation of the remaining terms (see Section 3D). This will also automatically take care of the nonspherical terms [limitation (*3*)]. We will also optimize both the superposition potential and the associated basis functions by varying the set $\{f^{\alpha}_{n,l}, Q^{\alpha}\}$ on the basis of the calculated crystal potential and charge density [limitation (*2*)]. Thus by relaxing limitation (*2*) we will eventually construct the "best" self-consistent atomic superposition potential, while in relaxing limitations (*1*) and (*3*) we will go beyond the superposition model to a fully self-consistent solution.

It is perhaps worth noting that the initial superposition potential employed in our scheme is already self-consistent with respect to the *variational basis set* employed in the crystal calculation [Equations (15) and (16)–(20)], since our numerical basis set [sets (a) and (b)] solves the one-site eigenvalue equations. This implies that if the superposition density $\rho^{\text{sup}}(\mathbf{r})$ comes very close to the crystal density (obtained from the band eigenstates), the model is approximately self-consistent. In other LCAO-type calculations the superposition potential is generally unrelated to the basis set, but rather to an independent atomic model (such as Hartree–Fock).

C. Matrix Elements and the Variational Problem

Having defined the variational basis set and the initial model crystal potential, we set up the LCAO variational equations for the solid in the usual way. Bloch crystal basis functions $\Phi_{\mu\alpha}(\mathbf{K},\mathbf{r})$ are constructed for each atomic-like orbital μ and inequivalent site α as

$$\Phi_{\mu\alpha}(\mathbf{K},\mathbf{r}) = N^{-1/2} \sum_{m}^{N} e^{i\mathbf{K}\mathbf{R}_m} \chi^{\alpha}_{\mu}(\mathbf{r} - \mathbf{R}_m - \mathbf{d}_{\alpha}) \tag{22}$$

where $\mathbf{K}$ labels the irreducible translational representation of the relevant space group and μ denotes collectively all atomic-like quantum numbers. The crystal eigenstate $\psi_j(\mathbf{K},\mathbf{r})$ belonging to the factor-group representation j is expanded in terms of the Bloch functions as

$$\psi_j(\mathbf{K},\mathbf{r}) = \sum_{\alpha=1}^{h} \sum_{\mu=1}^{\eta} C_{\mu\alpha j}(\mathbf{K}) \Phi_{\mu\alpha}(\mathbf{K},\mathbf{r}); \qquad j = 1, \cdots, h\eta \tag{23}$$

The secular $h\eta$ by $h\eta$ problem is defined for each $\mathbf{K}$ as

$$\sum_{\alpha=1}^{h} \sum_{\mu=1}^{\eta} [H_{\mu\alpha,\upsilon\beta}(\mathbf{K}) - S_{\mu\alpha,\upsilon\beta}(\mathbf{K}) \epsilon_j(\mathbf{K})] C_{\mu\alpha j}(\mathbf{K}) = 0 \tag{24}$$

where $H_{\mu\alpha,\upsilon\beta}$ and $S_{\mu\alpha,\upsilon\beta}$ are the Hamiltonian and overlap matrix elements in the Bloch function representation:

$$H_{\mu\alpha,\upsilon\beta} = \langle \Phi_{\mu\alpha}(\mathbf{K},\mathbf{r}) | V(\mathbf{r}) - \frac{1}{2}\nabla^2 | \Phi_{\upsilon\beta}(\mathbf{K},\mathbf{r}) \rangle \tag{25}$$

$$S_{\mu\alpha,\upsilon\beta} = \langle \Phi_{\mu\alpha}(\mathbf{K},\mathbf{r}) | \Phi_{\upsilon\beta}(\mathbf{K},\mathbf{r}) \rangle$$

and $\epsilon_j(\mathbf{K})$ denotes the one-electron band structure of crystal state j. Since our atomic-like basis functions $\chi^{\alpha}_{\mu}(\mathbf{r})$ are nonorthogonal on different sites, the matrix S is nondiagonal.

For many years the numerical implementation of LCAO-type first-principle calculations was severely hindered by the difficulties in computing matrix elements of the form (25). When the Bloch functions are written in terms of the atomic-like orbitals $\chi_{\mu}(\mathbf{r})$ and the

crystal potential is expanded into terms centered around the various atomic sites, many three-center integrals and crystal-field integrals have to be computed. The neglect of many of these integrals in most of the early LCAO calculations has been responsible for the misleading term "tight binding approximation" to general LCAO expansion techniques.

The matrix elements $H_{\mu\alpha,\upsilon\beta}(\mathbf{K})$ and $S_{\mu\alpha,\upsilon\beta}(\mathbf{K})$ are computed directly from the Bloch basis functions by using the Diophantine numerical integration scheme developed by Haselgrove [20] and Conroy [21] and adapted to molecular [22] and solid-state [23] calculations by Ellis and coworkers. The procedure involves defining a set of integration sampling coordinates $\{\mathbf{r}_i\}$ in the crystal unit cell, an associated set of weight functions $\{w_i\}$, and the use of the three-dimensional multicenter potential function $V(\mathbf{r}_i)$ and Bloch functions $\Phi_{\mu\alpha}(\mathbf{K},\mathbf{r}_i)$ in direct numerical form to obtain

$$\int\int\int d^3\mathbf{r}\Phi_{\mu\alpha}(\mathbf{K},\mathbf{r})V(\mathbf{r})\Phi_{\upsilon\beta}(\mathbf{K},\mathbf{r}) \cong \sum_{i=1}^{M} w_i\Phi_{\mu\alpha}(\mathbf{K},\mathbf{r}_i)V(\mathbf{r}_i)\Phi_{\upsilon\beta}(\mathbf{K},\mathbf{r}_i) \tag{26}$$

The convergence properties of the Diophantine scheme and the choice of numerical sampling points and weights have been the subject of numerous discussions in the literature [22, 23] and will not be repeated here. Using a numerical basis set as described above and 2000 sampling points, we obtain convergence of the valence bands of diamond to within 1 mRyd or less and convergence to within 2 mRyd for the first four conduction bands. A similar convergence is obtained for a typical transition-metal compound like TiS_2, using 4200 integration points.

In using the Diophantine integration scheme with our numerical basis set, several additional characteristics were revealed. Since the basis functions [sets (a) and (b) in 3A are chosen to be exact eigenstates of a given atomic-like one-center potential $g_\alpha(\mathbf{r})$ [Equation (12)], the crystal Hamiltonian operating on a Bloch state yields

$$H|\Phi_{\mu\alpha}(\mathbf{K},\mathbf{r})\rangle = (V_{\mathrm{SRC}}^{\mathrm{sup}}(\mathbf{r}) + V_{\mathrm{LRC}}^{\mathrm{sup}}(\mathbf{r}) + V_{\mathrm{ex}}^{\mathrm{sup}}(\mathbf{r}) + V_{\mathrm{corr}}^{\mathrm{sup}}(\mathbf{r})|\Phi_{\mu\alpha}(\mathbf{K},\mathbf{r})\rangle + \sum_m \{e^{i\mathbf{K}\mathbf{R}_m}$$

$$\chi_\mu^\alpha(\mathbf{r}-\mathbf{R}_m-\mathbf{d}_\alpha)[\epsilon_\mu - g_\alpha(\mathbf{r}-\mathbf{R}_m-\mathbf{d}_\alpha)]\} \equiv V|\Phi_{\mu\alpha}(\mathbf{K},\mathbf{r})\rangle + T|\Phi_{\mu\alpha}(\mathbf{K},\mathbf{r})\rangle \tag{27}$$

where ϵ_μ is the relevant atomic eigenvalue. In this scheme $V(\mathbf{r})|\Phi_{\mu\alpha}(\mathbf{K},\mathbf{r})\rangle$ and $T|\Phi_{\mu\alpha}(\mathbf{K},\mathbf{r})\rangle$ are combined numerically at each integration point $\mathbf{r}_i$ prior to integrating the Hamiltonian matrix elements $\langle\Phi|H|\Phi\rangle$. It is thus seen that the positive kinetic energy term [second term on the right-hand side of Equation (27)] is allowed to algebraically cancel the attractive potential term (first term on the right-hand side) before integration is attempted. Thus to the extent that the charge density derived from the μth atomic basis orbital contributes to the crystal ground-state potential, a great deal of numerical cancellation between large terms of opposite signs takes place [especially near the αth core in the solid, where the potential greatly resembles $g_\alpha(\mathbf{r})$] leaving finally a rather smooth $H\Phi$ function to be integrated. Note that a similar but arbitrary cancellation is the basis of the pseudopotential method and the cause of its success.

Since the exchange potential is treated no differently than the Coulomb potential, the cumbersome Fourier transform of $\rho(\mathbf{r})^{1/3}$ and the slowly convergent Fourier-series representation of the full core + valence charge density $\rho(\mathbf{r})$ needed in Fourier transform methods for computing LCAO matrix elements [24, 25] are avoided.

D. Self-Consistency

Although the superposition model potential [Equation (21)] is constructed in our scheme to be self-consistent with respect to the basis set, it is not self-consistent with

respect to the crystal eigenstates. The key problem in generating a refined crystal potential on the basis of the ground-state crystal charge density

$$\rho^{\text{cry}}(\mathbf{r}) = \sum_{\mathbf{K}} \sum_{j=1}^{\sigma_{\text{oc}}} \psi_j^*(\mathbf{K},\mathbf{r})\psi_j(\mathbf{K},\mathbf{r}) \tag{28}$$

is the solution of the three-dimensional multicenter Poisson equation associated with $\rho^{\text{cry}}(\mathbf{r})$. While the model superposition density [Equation (16)] is a sum of (radial) one-site terms [and hence the associated Poisson equation needed to determine $V_{\text{SRC}}^{\text{sup}}(\mathbf{r})$ is trivial], $\rho^{\text{cry}}(\mathbf{r})$ has only the totally symmetric factor group symmetry. Since the term "self consistency" has been used rather loosely in some previous band-structure calculations, we will discuss various possible degrees of self-consistency (SC) in what follows, along with the description of our own particular method to attain SC. We will thereby distinguish between charge and configuration self-consistency and full self-consistency.

(*a*) *Charge and configuration self-consistency.* The simplest way to avoid the integration of a multicenter Poisson equation associated with $\rho^{\text{cry}}(\mathbf{r})$ is obviously to expand the latter in terms of single-site functions. Having obtained the Coulomb potential in this form, one can recalculate the band structure. By charge and configuration self-consistency we mean a consistent relation between the crystal potential and the crystal charge density via the Poisson equation (for the Coulomb part) and the exchange and correlation functions $F_{\text{ex}}[\rho(\mathbf{r})]$ $F_{\text{corr}}[(\mathbf{r})]$, respectively, *in which we limit the crystal density to sums of one-center terms located on atomic sites.*

As indicated previously, depending on the various degrees of approximation involved in simulating the crystal density $\rho^{\text{cry}}(\mathbf{r})$ by a superposition density

$$\rho^{\text{sup}}(\mathbf{r}) = \sum_{m=1}^{N} \sum_{\alpha=1}^{h} \left\{ \sum_i a_i \rho_i(\mathbf{r} - \mathbf{R}_m - \mathbf{d}_\alpha) \right\} \tag{29}$$

there will exist a residual density $\Delta\rho(\mathbf{r}) \equiv \rho^{\text{cry}}(\mathbf{r}) - \rho^{\text{sup}}(\mathbf{r})$ that is not amenable to fitting by a single-site basis located on atomic sites. In Equation (29) a_i and ρ_i denote the expansion coefficients and the fitting functions, respectively. A great deal of charge and configuration self-consistent calculations on molecular and solid-state systems are based on various modifications to the form (29). Thus the multiple-scattering $X\alpha$ (MS-$X\alpha$) method [17] projects the crystal density $\rho^{\text{cry}}(\mathbf{r})$ onto a muffin-tin single-site spherical basis, the LCAO-$X\alpha$ method of Sambe and Felton [19a] uses contracted Gaussians for $\rho_i(\mathbf{r})$, the LCAO band approach of Chaney and coworkers [18] replaces $\rho_i(\mathbf{r})$ by angular dependent function of the $C_{lm}(r)Y_{lm}(\theta,\Phi)$ type, the molecular discrete-variational method (DVM) of Ellis and coworkers [22a] and various forms of the iterative extended Hückel (IEXH) method [26] use for a_i the Mulliken or Löwdin population of the states $\{\psi_i(\mathbf{r}), i = 1, \cdots, \sigma_{\text{oc}}\}$ and atomic-like densities for $\rho_i(\mathbf{r})$, and so forth. Since in all of these methods $\Delta\rho(\mathbf{r})$ is neglected and convergence is examined only with respect to the restricted form, the only valid way to estimate the quality of the converged results is by evaluating the residual $\Delta\rho(\mathbf{r})$ and its possible effects on the final results. Unfortunately, this has hardly ever been done in these calculations. It is thus important to realize that when convergence is obtained under these circumstances, the result corresponds to a given self-consistent solution under a particular choice of partitioning the multicenter density into single-site (spherical) terms (neglecting the residual $\Delta\rho(\mathbf{r})$. One would thus hardly expect the converged results, obtained by a Mulliken partitioning of charge, to resemble those obtained by Gaussian basis fit functions, etc. Since there exists an unlimited number of ways of partitioning $\rho^{\text{cry}}(\mathbf{r})$ into lattice sums of one-site terms [the final goal of charge and configuration self-consistency being to minimize $\Delta\rho(\mathbf{r})$ over space], the only relevant

criterion for chosing a partitioning scheme seems to be efficiency in representing $\rho^{cry}(\mathbf{r})$ and a possible physical significance of the projection set. Our particular choice of partitioning scheme is just the population-dependent atomic superposition density:

$$\rho^{sup}(\mathbf{r}) = \sum_{m=1}^{N} \sum_{\alpha=1}^{h} \sum_{n,l}^{N_{oc}} f_{n,l} \left[\chi^{\alpha}_{n,l}(\mathbf{r} - \mathbf{R}_m - \mathbf{d}_\alpha; \{f^{\alpha}_{n'l'}, Q^{\alpha}\})\right]^2 \tag{30}$$

We will thus vary the crystalline potential and the variational basis set $\chi^{\alpha}_{n,l}(\mathbf{r})$, by changing iteratively the population numbers $f^{\alpha}_{n,l}$ and the atomic (ionic) charges Q^{α} to minimize in a least squares sense the deviation

$$\sigma^2 \equiv \frac{1}{\Omega} \int \Delta\rho(\mathbf{r})^2 d\mathbf{r} \tag{31}$$

The main reasons for this choice are as follows.

(*1*) Using this choice we retain the self-consistency between the crystal potential and the basis set at each iteration state. Thus both the basis set and the crystal potential will be completely defined by the set $\{f^{\alpha}_{n,l}, Q^{\alpha}\}$ with no extra auxiliary basis functions. Aside from computational convenience in keeping a single functional set; this is, admittedly, just an aesthetic argument.

(*2*) To provide a natural way to perform, aside from a linear variation (by solving the secular equations), also a nonlinear variation on the basis set. We will thus resolve the atomic-like equation (12) for each atom in the unit cell at each (or every several) iteration(s), using a new $\{f^{\alpha}_{n,l}, Q^{\alpha}\}$ set determined by the requirement that the resulting superposition charge density be close to the obtained crystal density in a least squares sense. As it turns out, a nonlinear variation of the basis set proved to be necessary only when substantial fractional electronic populations were promoted into previously unpopulated (virtual) orbitals. Under these circumstances recalculation of the atomic self-consistent orbitals yielded much more contracted orbitals for the formerly virtual states, thus rendering them useful in the crystalline variational calculation. By contrast, ordinary atomic virtual orbitals are discarded from the basis set when linear-dependence problems caused by their diffuse nature become severe. Since such charge promotions do not occur in every iteration, it is necessary to regenerate an optimized numerical set only after several iterations.

(*3*) To be able to select among all possible solutions of an atomic-like Hamiltonian of the form given in Equation (12), the best superposition potential (in the least squares sense) and the associated atomic-like basis functions, to be used in future non-self-consistent calculations within the superposition model.

(*4*) To prepare the residual $\Delta\rho(\mathbf{r})$ [obtained after step (a) in the self-consistency has been completed] in a way best suited for "full" self-consistency [step (b) in self-consistency]. This will be discussed in some detail in the next section.

In performing step (a) of self-consistency, we compute in a general iteration the basis functions $\{\chi^{\alpha}_{\mu}(\mathbf{r})\}$ [Equation (12)] and the superposition Coulomb potential $V^{sup}_{SRC}(\mathbf{r})$, $V^{sup}_{LRC}(\mathbf{r})$ [Equations (17) and (18)] for an assumed set $\{f^{\alpha}_{n,l}, Q^{\alpha}\}$ and use the crystal density obtained from the previous iteration to compute $F_{ex}[\rho^{cry}(\mathbf{r})]$ and $F_{corr}[\rho^{cry}(\mathbf{r})]$. Having obtained a new set of basis functions and a new potential, the band problem is repeated to yield a new crystal density calculated from all occupied bands at a limited number of $\mathbf{K}$ points in the Brillouin zone. In the present calculation we determine $\rho^{cry}(\mathbf{r})$ using the six nearest volume points for the face-centered cubic lattice [27]. This seems to be sufficient to obtain the charge density with reasonable accuracy for insulating systems like those treated here [27, 28]. Different prescriptions for choosing a small number of

TABLE I. Standard deviation $\sigma(e)$ [Equation (31)] measuring the average number of electrons that are 'misplaced' in the superposition model for the crystal charge density before and after charge and configuration self-consistency.

System and No. of Electrons per cell	Initial Configuration	Non-Self Consistent $\sigma(e)$	Self-Consistent $\sigma(e)$
Diamond, 12e	C:$1s^2 2s^2 2p^2$	0.1534	0.098
Cubic BN, 12e	B:$1s^2 2s^2 2p^1$ N:$1s^2 2s^2 2p^3$	0.2951	0.101
LiF, 12e	L:$1s^2 2s^1$ F:$1s^2 2s^2 2p^5$	0.2279	0.090
Ne, 10e	Ne:$1s^2 2s^2 2p^6$	0.003	0.003

points to be used in efficiently representing the average of a periodic function, like $\rho(\mathbf{r})$, over the Brillouin zone [29, 30] are presently being tested. Having chosen insulating and semiconducting systems to work on, relieves us presently from the necessity of recalculating the Fermi energy at each iteration. Typical results for the standard deviation σ obtained during the iteration history in step (a) of self-consistency are shown in Table I. Generally, three to eight iterations were needed to obtain these results.

(*b*) *Full self-consistency.* Although it proved possible in some systems to carry out step (a) of self-consistency so that the final $\Delta\rho(\mathbf{r})$ is made to be very small (in which case an essentially self-consistent result is obtained, see [18] and the Ne results shown in Table I], it is desirable to provide a general scheme for treating the full density $\rho^{\text{cry}}(\mathbf{r}) = \rho^{\text{sup}}(\mathbf{r}) + \Delta\rho(\mathbf{r})$ self-consistently in cases where the complete crystal density $\rho^{\text{cry}}(\mathbf{r})$ cannot be effectively projected into an atomic-centered expansion. In order to illustrate our method of obtaining step (b) of self-consistency, we will discuss first some aspects of the results obtained in step (a).

The solid lines in Figures 1 and 2 show the function $\Delta\rho(\mathbf{r})$ obtained in the first iteration of the charge and configuration self-consistency for boron-nitride and diamond, respectively, plotted along the bonding [111] direction. The assumed electronic configuration in the superposition models was $1s^2 2s^2 2p^q$, where q = 1,2,3 for boron, carbon, and nitrogen, respectively. It is seen that aside from a buildup in the crystal density relative to the atomic superposition density in the interatomic region (indicating covalent bond formation), the function $\Delta\rho(\mathbf{r})$ is also characterized by some rather sharp features, localized near the atomic sites. Similar features have been identified by Lubinsky and coworkers [31] in their non-self-consistent calculation on SiC (see [31, fig. 5]). The dashed curves in Figures 1 and 2 show the $\Delta\rho(\mathbf{r})$ functions for boron-nitride and diamond, as obtained at the convergence limit of charge and configuration self-consistency. It is observed that the sharp localized features near the atomic sites are almost entirely eliminated, while the interatomic bond charge buildup still persists. This would indicate that in carrying out charge and configuration self-consistency to convergence, we have effectively accounted for the bonding effects originating from intraatomic charge redistribution, while the interatomic bond formation is largely not amenable to an atomic

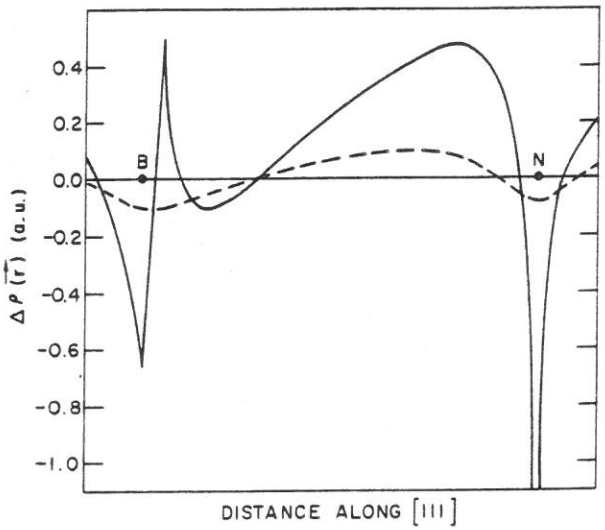

Figure 1. Comparison of the charge density difference $\Delta\rho(\mathbf{r})$ for boron nitride, calculated along the bonding [111] direction, between the zeroth iteration (solid curve) and the final iteration (dashed curve) in the charge and configuration self-consistency.

superposition model description even after the latter is optimized with respect to the population numbers in a least squares sense. The function $\Delta\rho(\mathbf{r})$ obtained at the final iteration of the charge and configuration self-consistency, called the residual $\Delta\rho(\mathbf{r})$, has the following properties.

(*1*) It encloses zero charge since by construction

$$\int \Delta\rho(\mathbf{r})d\mathbf{r} = 0 \tag{32}$$

(*2*) It is minimized over the unit cell space (through the least square procedure using the numerical atomic fit functions); thus

$$\int \Delta\rho(\mathbf{r})^2 d\mathbf{r} = \min \tag{33}$$

(*3*) It is a smooth function of space coordinates [this can be controlled, if so desired, by performing the least squares fitting in Equations (30) and (31) in a weighted form].

These properties of the residual $\Delta\rho(\mathbf{r})$ make it particularly suitable for a rapidly convergent Fourier series representation. We thus proceed in step (b) of self-consistency by calculating the Fourier transform $\Delta\rho(\mathbf{K}_s)$ over a set of reciprocal lattice vectors (RLV) $\mathbf{K}_s$ (using a Diophantine three-dimensional integration):

$$\Delta\rho(\mathbf{K}_s) = \frac{1}{\Omega}\int e^{-i\mathbf{K}_s\cdot\mathbf{r}}\Delta\rho(\mathbf{r})d\mathbf{r} \tag{34}$$

where Ω is the unit cell volume. The Coulomb potential associated with $\Delta\rho(\mathbf{r})$ is thus simply given by

$$\Delta V_{\text{co}}(\mathbf{r}) = \sum_{K_s\neq 0} -4\pi\frac{\Delta\rho(\mathbf{K}_s)}{K_s^2}e^{-i\mathbf{K}_s\cdot\mathbf{r}} \tag{35}$$

The term $\mathbf{K}_s = 0$ is excluded due to condition (32). The sum over the RLVs is rapidly

convergent both due to the smooth form of $\Delta\rho(\mathbf{r})$ and due to the additional K_s^{-2} factor in Equation (35). The exchange and correlation potentials are simply given by

$$V_{ex}(\mathbf{r}) = F_{ex}[\rho^{sup}(\mathbf{r}) + \Delta\rho(\mathbf{r})]$$
$$V_{corr}(\mathbf{r}) = F_{corr}[\rho^{sup}(\mathbf{r}) + \Delta\rho(\mathbf{r})] \tag{36}$$

The solution of the band structure is then repeated with the new potential

$$V_{cry}(\mathbf{r}) = V_{SRC}^{sup}(\mathbf{r}) + \Delta V_{co}(\mathbf{r}) + V_{LRC}(\mathbf{r}) + V_{ex}(\mathbf{r}) + V_{corr}(\mathbf{r}) \tag{37}$$

The resulting charge density is used to compute a new $\Delta\rho(\mathbf{r})$ and $\Delta\rho(\mathbf{K}_s)$, and the iterations are continued until the relative change in the Fourier components $\Delta\rho(\mathbf{K}_s)$ in successive iterations is smaller than a prescribed tolerance [usually 10^{-5} in $\Delta\rho(111)$]. If the first step of self-consistency is properly carried out, only a few iterations are required in step (b) (for example, two to four for diamond) and only the first few stars (5–10) are

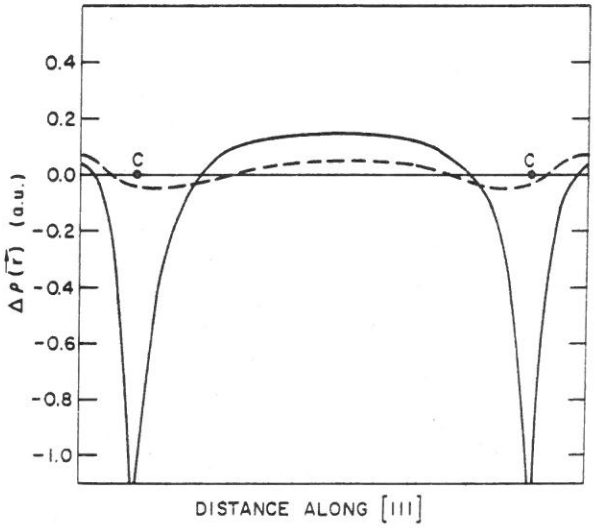

Figure 2. Comparison of the charge density difference $\Delta\rho(\mathbf{r})$ for diamond, calculated along the bonding [111] direction, between the zeroth iteration (solid curve) and the final iteration (dashed curve) in the charge and configuration self-consistency.

required in the expansion (35). $\Delta\rho(\mathbf{K}_s)$ for higher numbers of RLVs reflects the residual core difference charge, and is hence negligibly small since it has been absorbed in $\rho^{sup}(\mathbf{r})$ in step (a) of self-consistency. It is noted that in the described method slowly convergent Fourier series resulting from transforming the full core + valence density [24, 25] are completely avoided as are the cumbersome integrals resulting from a Fourier transform of $\rho(\mathbf{r})^{1/3}$ that appear in schemes that compute the iterated exchange potential [Equation (36)] in reciprocal rather than in real space.

Our self-consistent band approach thus combines the flexibility in handling general basis functions and crystal potentials (offered by the Diophantine integration scheme as applied to LCAO matrix elements in the Bloch representation) with convenience in handling charge density terms that are not amenable to a superposition representation (offered by the Fourier transform approach). In what follows we will illustrate some examples for the results obtained to date with the above-described method.

4. Illustrative Results on Diamond

To illustrate the performance of the method described above we describe some results obtained for diamond. Although a great deal of theoretical work has been done on the electronic structure of diamond within the local exchange formalism (among others we note the APW work of Keown [32] and Neto and Ferreira [16b], the OPW work of Bassani and Yoshimine [16a], the OPW pseudopotential work of Kleinman and Phillips [33], and the LCAO work of Painter, Ellis, and Lubinsky [34]), none of these were carried to self consistency. To illustrate the various levels of self-consistency one might obtain in this problem, we have carried out step (a) of self-consistency in three different ways.

(*1*) The crystal charge $\rho^{\text{cry}}(\mathbf{r})$ is partitioned at each iteration step into a superposition density $\rho^{\text{sup}}(\mathbf{r})$ using a Mulliken population analysis:

$$\rho^{\text{sup}}_{\text{MUL}}(\mathbf{r}) = \sum_{m=1}^{N} \sum_{\alpha=1}^{h} \sum_{n,l} M^{\alpha}_{n,l} \cdot [\chi^{\alpha}_{n,l}(\mathbf{r} - \mathbf{R}_m - \mathbf{d}_{\alpha}; \{M^{\alpha}_{n'l'}, Q^{\alpha}\})]^2 \tag{38}$$

where $M^{\alpha}_{n,l}$ is the Mulliken gross-atomic population [35] of all occupied states contribution to the n,l,α basis function. Having determined $M^{\alpha}_{n,l}$ (by adding the contributions from all occupied bands and averaging over the six special **K** points mentioned in Section 3D), we compute the superposition short-range Coulomb potential arising from $\rho^{\text{sup}}_{\text{MUL}}(\mathbf{r})$ [Equation (17)] while the exchange and correlation potentials [Equations (19) and (20)] are computed directly from $\rho^{\text{cry}}(\mathbf{r})$. The solution of the band structure is repeated until the populations $M^{\alpha}_{n,l}$ calculated from successive iterations agree to within 10^{-3} e. At the final iteration we compute the standard deviation σ_{MUL} according to Equation (31).

(*2*) The same procedure is repeated using the Löwdin populations $L^{\alpha}_{n,l}$ [36] during the iteration process. At the final iteration we compute $\sigma_{\text{LÖW}}$.

(*3*) The third method of carrying out the charge and configuration self-consistency is by simply using the superposition model given in Equation (30), where the population numbers $f^{\alpha}_{n,l}$ are allowed to change freely so as to minimize the squared deviation σ [Equation (31)]. The final σ value obtained in this calculation is denoted by σ_{MIN}.

All three calculations were performed at a lattice constant of 3.5669 Å using a minimal numeric set of $1s$, $2s$, and $2p$ orbitals with no correlation added and 2000 integration points. In each case the basis functions were nonlinearly optimized at every iteration. The results are summarized in Table II. It is immediately recognized that although convergence in the populations (and eigenvalues) can be readily achieved using either the Mulliken or the Löwdin partitioning of the total charge density, the self-consistent results obtained by these schemes do not minimize the deviation between the superposition charge and the crystalline charge as obtained directly from the eigenvectors. Furthermore, the "converged" results differ markedly from each other (a $2p$ to $2s$ hybridization population ratio of 2.77 in the Mulliken case and 3.83 in the Löwdin case) and from the minimum deviation results (a hybridization ratio of 1.70). Although in this case the Mulliken prescription seems to be somewhat more efficient in lowering the charge deviation than is a Löwdin scheme ($\sigma_{\text{MUL}} < \sigma_{\text{LÖW}}$), both methods are rather inadequate for obtaining true charge and configuration self-consistency. It is also to be noted that even a direct minimization technique yields a rather large residual charge difference (1.22% of the 8 valence electrons or 0.82% of the total of 12 core + valence electrons are misplaced, on the average, by the "best" superposition density). This indicates the need to incorporate the density terms that are not amenable to a superposition representation in a fully self-consistent treatment. The details of the full self-consistency treatment in

TABLE II. Self-consistent electronic populations and final standard deviations as obtained by iterating on Mülliken charges, Löwdin charges, and through a direct minimization method.

	1s(e)	2s(e)	2p(e)	σ(e)
SC Mulliken Populations	2.000	1.062	2.938	0.1595
SC Löwdin Populations	1.999	0.939	3.060	0.1895
Free Minimization	2.000	1.482	2.519	0.098

diamond will be given elsewhere. Here we discuss some of our results and compare them with those obtained by the restricted Hartree–Fock treatment of Euwema and coworkers [4a, 37].

Table III shows the calculated X-ray structure factors for some of the lowest h,k,l reflections in diamond, as obtained as a convergence limit of the full self-consistency iteration treatment, using a numerical basis set of $1s$, $2s$, $2p$, $3s$, $3p$, and $3d$ for carbon [sets (a) + (b), Section 3A]. The results are compared with experiment [38, 39] and with the Hartree–Fock results of Euwema and coworkers [37]. It is seen that the local density formalism predicts the ground-state charge density in diamond rather well. In particular, the weak 222 forbidden reflection that arises only from the contribution of the "bonding" charge (a superposition charge would yield exactly zero for that reflection) is reproduced remarkably well. The 222 form factor, as calculated by a minimal numeric set (the calculation being carried to full self-consistency), is only 0.076, indicating the importance of including virtual states even in ground-state bonding. In view of this sensitivity of the structure factor to an increase in the basis set, it would seem that the Hartree–Fock results would come into closer agreement with experiment, if some polarization functions were included into the s–p Gaussian set.

The results for the form factor with exchange and correlation (Table III, column 4) show a somewhat larger form factor as compared to the calculation with exchange only (column 3), indicating a contraction in the density. The effect, as can be seen from the table, is rather small and no conclusion as to the importance of the correlation term seems to be possible in this case. Calculations of the Compton profile of diamond are underway.

TABLE III. Comparison between experimental and calculated structure factors for diamond. $\rho(0,0,0)$ is normalized to six electrons.

Reflection	Exp [38]	Present Work Exchange Only	Present Work Exchange + Correlation	HF [37]
111	3.32	3.273	3.280	3.30
220	1.98	1.992	1.995	1.93
311	1.66	1.720	1.722	1.67
222	0.144±0.015*	0.137	0.139	0.08
400	1.48	1.494	1.493	1.55

*Measured by Renninger Ref. [39].

These will serve to further check the predictions of the local density formalism of the ground-state wave functions.

We next discuss the cohesive energy of diamond which is measured to be 7.6 eV/atom [10]. The Hartree–Fock results for the binding energy lie between 4.6 and 5.0 eV, depending on the various calculation parameters in the s–p Gaussian set [37]. The details of calculation of the crystal total energy under the LDF formalism are given in the Appendix. The total energy of the free carbon atom is calculated in a non-spin-polarized fashion* using the direct numerical integration scheme of Herman and Skillman [41]. The binding energy of diamond using a minimal numeric set with no correlation effects included (6300 integration points, $\alpha = 2/3$) is 5.17 eV, and the virial ratio $-2\text{KE}/\text{PE}$ is 1.0023. When the same calculation is repeated using the correlation functional in the potential [Equation (20)] and total energy expression [Equation (9)] for both the atom and the crystal, a binding energy of 10.46 eV is revealed. In this case the virial theorem does not hold any longer due to the different scaling of the correlation functional as compared with the exchange functional (compare [42]). The no-correlation calculation is repeated with a minimal numeric set augmented by free Slater orbitals of $3s$ and $3p$ symmetry (with Slater exponents of 1.4 and 2.642, respectively). This yields a virial constant of 1.0021 and a binding energy of 5.21 eV. The major improvement in the calculated binding energy is brought about by the inclusion of an ion pair into the basis set [set (c) in Section 3A] in addition to the neutral carbon minimal numeric set. Inclusion of this set yields a virial ratio of 1.0004 and a binding energy of 7.29 eV (11.92 eV is obtained when correlation is included). Calculations of the cohesive energy are usually very tedious due to the need to use a large number of integration points in order to maintain reasonable accuracy in the various integrals involved [Equations (45), (50), and (51)]. Even with the large number of integration points used in this work, the accuracy of the binding energy is estimated to be no better than 0.15 eV. Further calculations are planned to obtain the equilibrium lattice constant in diamond. The fact that the virial ratio obtained in a calculation at the experimental lattice constant is very close to unity, would indicate that the theoretical equilibrium lattice parameter would be in close agreement with experiment.

Judging from the calculated structure factors and binding energies, it would thus seem that both the Hartree–Fock and the local density formalism are capable of yielding good results for ground-state observables. The differences between the quality of the various basis sets used are perhaps more significant than the different treatment of the exchange in the two methods.

Appendix

Calculation of the Total Energy

The calculation of the total energy per unit cell of an infinite solid is fraught by the well-known difficulties of the divergency in the individual electron–electron, electron–nuclear, and nuclear–nuclear terms and by the need to perform very accurate three-dimensional integrals on numerical forms of the potential. This problem has been treated previously by De Cicco [43] and Rudge [44] in a form that is mainly suitable for a muffin-tin partitioning of the potential (in which the three-dimensional integrals are reduced to radical one-dimensional integrals). For the sake of convenience, we repeat the derivation for a general form of the potential.

* Spin-polarization corrections to the atomic total energy are being calculated.

The total ground-state energy, in the LDF formalism, is given by the total electronic energy [Equation (9)] plus the nuclear–nuclear repulsion term:

$$V_{\mathrm{nn}} = \sum_{\substack{n\alpha \\ m\alpha \neq n\beta}} \sum_{m\beta} \frac{Z_\alpha Z_\beta}{|\mathbf{R}_n + \mathbf{d}_\alpha - \mathbf{R}_m - \mathbf{d}_\beta|} \tag{39}$$

We use the following notation for the various potential terms. The electron–nuclear potential $V_{\mathrm{en}}(\mathbf{r})$ is given by

$$V_{\mathrm{en}}(\mathbf{r}) = -\sum_{m,\alpha} \frac{Z_\alpha}{|\mathbf{R}_m - \mathbf{d}_\alpha - \mathbf{r}|} \tag{40}$$

the electron–electron potential $V_{\mathrm{ee}}(\mathbf{r})$ is

$$V_{\mathrm{ee}}(\mathbf{r}) = \int d\mathbf{r}' \frac{\rho(\mathbf{r}')}{|\mathbf{r} - \mathbf{r}'|} \tag{41}$$

and the exchange potential $V_{\mathrm{ex}}(\mathbf{r})$ is

$$V_{\mathrm{ex}}(\mathbf{r}) = -\frac{3}{4}\left(\frac{3}{\pi}\rho(\mathbf{r})\right)^{1/3} \tag{42}$$

and a similar equation for the correlation potential $V_{\mathrm{corr}}(\mathbf{r})$, based on the definition (8). In terms of these quantities, the total electron plus nuclear energy is given as

$$E_{\mathrm{tot}} = \mathrm{KE} + \int \rho(\mathbf{r}) \left[V_{\mathrm{en}}(\mathbf{r}) + \frac{1}{2} V_{\mathrm{ee}}(\mathbf{r}) + V_{\mathrm{ex}}(\mathbf{r}) + V_{\mathrm{corr}}(\mathbf{r}) \right] d\mathbf{r} + V_{\mathrm{nn}} \tag{43}$$

The kinetic energy term KE is given usually by the direct expression, using the crystal eigenvectors ψ_j:

$$\mathrm{KE} = \sum_j \left\langle \psi_j(\mathbf{r}) \middle| -\frac{1}{2}\nabla^2 \middle| \psi_j(\mathbf{r}) \right\rangle \tag{44}$$

where the sum is over all occupied states in the Brillouin zone. Alternatively, using the fact that ψ_j is an exact eigenfunction [Equation (3)] of $-1/2\,\nabla^2 + [V_{\mathrm{ne}}(\mathbf{r}) + V_{\mathrm{ee}}(\mathbf{r}) + 4/3\,V_{\mathrm{ex}}(\mathbf{r}) + V_{\mathrm{corr}}(\mathbf{r})]$, the KE might be equivalently calculated from

$$\mathrm{KE} = \sum_j \epsilon_j - \int \rho(\mathbf{r}) \left[V_{\mathrm{ne}}(\mathbf{r}) + V_{\mathrm{ee}}(\mathbf{r}) + \frac{4}{3} V_{\mathrm{ex}}(\mathbf{r}) + V_{\mathrm{corr}}(\mathbf{r}) \right] d\mathbf{r} \tag{45}$$

We next modify the potential energy appearing as the second term in Equation (43), recognizing that V_{en}/N, V_{ee}/N, and V_{nn}/N are divergent as N goes to infinity. We thus partition the potential energy in the following form:

$$\mathrm{PE} = \frac{1}{2}\int \rho(\mathbf{r})[V_{\mathrm{ne}}(\mathbf{r}) + V_{\mathrm{ee}}(\mathbf{r})]d\mathbf{r} + \left[\frac{1}{2}\int \rho(\mathbf{r}) V_{\mathrm{ne}}(\mathbf{r}) d\mathbf{r} + V_{\mathrm{nn}}\right] + \int \rho(\mathbf{r})[V_{\mathrm{ex}}(\mathbf{r}) + V_{\mathrm{corr}}(\mathbf{r})]d\mathbf{r} \tag{46}$$

In this form divergencies in the individual terms are grouped to yield three finite terms, each linear in N, so that a total energy per cell, E/N, can be defined. The two first terms in Equation (46) represent the total electrostatic energy in the system, E_{elec}, and are given by

$$E_{\text{elec}} = \frac{1}{2}\int_{\text{uc}}\int_{\infty} d\mathbf{r}d\mathbf{r}'|\mathbf{r}-\mathbf{r}'|^{-1}\left[\rho(\mathbf{r}) + \sum_{n,\alpha} Z_\alpha \delta^3(\mathbf{r}-\mathbf{R}_n-\mathbf{d}_\alpha)\right] \times \left[\rho(\mathbf{r}') + \sum_{m,\beta}{}' Z_\beta \delta^3(\mathbf{r}'-\mathbf{R}_m-\mathbf{d}_\beta)\right] \quad (47)$$

Each term in the square brackets in Equation (47) represents the total electronic + nuclear charge, and the prime on the second sum indicates exclusion of the self-interaction $\alpha = \beta, n = m$ term. The electrostatic energy can be written in terms of a Coulomb electronic potential

$$V_c(\mathbf{r}) = V_{\text{ee}}(\mathbf{r}) + V_{\text{en}}(\mathbf{r}) = \int_{\infty} d\mathbf{r}'|\mathbf{r}-\mathbf{r}'|^{-1}\left[\rho(\mathbf{r}') + \sum_{n,\alpha} Z_\alpha \delta^3(\mathbf{r}'-\mathbf{R}_n-\mathbf{d}_\alpha)\right] \quad (48)$$

in the following way:

$$E_{\text{elec}} = \frac{1}{2}\int \rho(\mathbf{r})V_c(\mathbf{r})d\mathbf{r} + \frac{1}{2}\sum_n \int_{\text{uc}} \sum_\alpha Z_\alpha \delta^3(\mathbf{r}-\mathbf{R}_n-\mathbf{d}_\alpha) \times \left\{\int_{\infty} |\mathbf{r}-\mathbf{r}'|^{-1}\left[\rho(\mathbf{r}') + \sum_{m\beta\neq n\alpha} Z_\beta \delta^3(\mathbf{r}'-\mathbf{R}_m-\mathbf{d}_\beta)\right]\right\} d\mathbf{r} \quad (49)$$

The first term in Equation (49) is just the first term in Equation (46). The term in curly brackets represents the sum of the electron–nuclear potential at site α due to all nuclei except the nucleus α, plus the electron–electron potential. To simplify its form, we first calculate the total electrostatic potential at site α due to all charges (electron and nuclear) except the αth nucleus itself, and add to it the electron–electron potential at site α that was omitted in the previous term. We thus obtain

$$E_{\text{elec}} = \frac{1}{2}\int \rho(\mathbf{r})V_c(\mathbf{r})d\mathbf{r} + \frac{1}{2}\sum_n \int_{\text{uc}} \sum_\alpha Z_\alpha [V_{\text{vac}}^{(\alpha)} + V_{\text{ee}}(\mathbf{r}-\mathbf{R}_m-\mathbf{d}_\alpha)]\delta^3(\mathbf{r}-\mathbf{R}_{n\alpha}) \quad (50)$$

where the "vacancy electrostatic potential" at site α, $V_{\text{vac}}(\alpha)$ is

$$V_{\text{vac}}(\alpha) = \sum_{m\beta\neq n\alpha} V_{\text{ee}}(\mathbf{r}-\mathbf{R}_m-\mathbf{d}_\beta) + V_{\text{en}}(\mathbf{r}-\mathbf{R}_m-\mathbf{d}_\beta) \quad (51)$$

Performing the trivial integrations yields

$$E_{\text{elec}} = \frac{1}{2}\int \rho(\mathbf{r})V_c(\mathbf{r})d\mathbf{r} + \frac{1}{2}\sum_\alpha Z_\alpha [V_{\text{vac}}(\alpha) + V_{\text{ee}}(\alpha)] \quad (52)$$

The potential energy is thus given by

$$\text{PE} = E_{\text{elec}} + \int \rho(\mathbf{r})[V_{\text{ex}}(\mathbf{r}) + V_{\text{corr}}(\mathbf{r})]d\mathbf{r} \quad (53)$$

The individual terms in Equations (50) and (51) are readily calculated by performing three-dimensional Diophantine integrations. The convergence is usually rather slow, and a large number of points (6000–10,000) have to be used to obtain stable results for the cohesive energy.

It should be noted that the potential terms appearing in the kinetic-energy equation (45) can be any *input* model potential that was used to solve the eigenvalue problem

[Equation (3)], while the potential terms appearing in Equations (50) and (51) correspond to those obtained from the *crystal charge density*. These two types of potential terms are thus equivalent only at the limit of full self-consistency. One should also note that the Coulomb potential terms calculated from the crystal density (by solving the associated Poisson equation) might contain an arbitrary integration constant. However, this constant is canceled in performing the sum in Equation (50). The calculation of the ground-state energy of isolated atoms (or ions) to be used along with the crystal total energy per cell to compute the cohesive energy is performed in the usual way, described in other references in detail (for example, [41]).

Acknowledgment

The authors are greatly indebted to D. E. Ellis for helpful collaboration in the early stages of this work and for making available the early non-self-consistent DVM programs. They are grateful to R. Kautz and F. Averill for stimulating discussions on the total energy problem.

This work was supported by the National Science Foundation and the Air Force Office of Scientific Research.

Bibliography

[1] P. Hohenberg and W. Kohn, Phys. Rev. **B136,** 864 (1964).
[2] G. S. Painter and D. E. Ellis, in *Computational Methods in Band Theory,* P. M. Marcus, J. F. Janak, and A. R. Williams, Ed. (Plenum Press, New York 1971), p. 276.
[3] A. B. Kunz and D. J. Mickish, Phys. Rev. **B8,** 779 (1973); J. Phys. **C6,** 1723 (1973).
[4] (a) R. N. Euwema, G. G. Wepfer, O. T. Surratt, and D. L. Wilhite, Phys. Rev. **B7,** 818 (1973); **B9,** 5249 (1973); (b) F. E. Harris and H. J. Monkhorst, *Computational Methods in Band Theory,* P. M. Marcus, J. F. Janak, and A. R. Williams, Eds. (Plenum Press, New York, 1971), p. 517.
[5] W. Kohn and L. J. Sham, Phys. Rev. **A140,** 1133 (1965).
[6] M. Rasolt and D. J. W. Geldart, Phys. Rev. Lett. **35,** 1234 (1975).
[7] L. Hedin and B. J. Lundqvist, J. Phys. **C4,** 2064 (1971).
[8] K. S. Singwi, A. Sjölander, M. P. Tosi, and R. H. Land, Phys. Rev. **B1,** 1044 (1970).
[9] B. Y. Tong, Phys. Rev. **B6,** 1189 (1972).
[10] O. Gunnarsson, P. Johansson, S. Lundqvist, and B. I. Lundqvist, INT/ J. Quant. Chem. **S9,** 83 (1975).
[11] R. Latter, Phys. Rev. **99,** 510 (1955).
[12] D. E. Ellis and F. Averill, J. Chem. Phys. **60,** 2856 (1974).
[13] W. H. Adams, J. Chem. Phys. **34,** 89 (1961); **37,** 2009 (1967); T. L. Gilbert, in *Molecular Orbitals in Chemistry, Physics and Biology,* P. O. Löwdin, Ed. (Academic Press, New York, 1964).
[14] D. E. Ellis, A. Rosen, and P. F. Walch, Int. J. Quant. Chem. **S9,** 351 (1975).
[15] P. P. Ewald, Ann. Physik **64,** 753 (1971). See also M. P. Tosi, in *Solid State Physics,* Vol. 16, F. Seitz and B. Turnbull, Eds. (Academic Press, New York, 1964), p. 1.
[16] (a) F. Bassani and M. Yoshimine, Phys. Rev. **130,** 20 (1963); (b) J. R. P. Neto and L. G. Ferreira, J. Phys. **C6,** 3430 (1973); (c) E. Lafon, M.I.T. Solid State and Molecular Theory Group Reports, Rep 69, p. 66, 1968.
[17] K. H. Johnson and F. C. Smith, Jr., in *Computational Methods in Band Theory* P. M. Marcus, J. F. Janak, and A. R. Williams, Eds. (Plenum Press, New York, 1971), p. 377.
[18] R. C. Chaney, E. E. Lafon, and C. C. Lin, Phys. Rev. **B4,** 2734 (1971).
[19] (a) H. Sambe and R. H. Felton, J. Chem. Phys. **62,** 1122 (1975); (b) E. J. Baerends and P. Ros, Chem. Phys. Lett. **2,** 41, (1973).
[20] C. B. Haselgrove, Math. Comp. **15,** 373 (1961).
[21] H. J. Conroy, J. Chem. Phys. **47,** 5307 (1967).
[22] (a) E. J. Baerends, D. E. Ellis, and P. Ros. Theor. Chim. Acta **27,** 339 (1972); (b) A. J. Freeman and D. E. Ellis, Phys. Rev. Lett. **24,** 516 (1970); (c) D. E. Ellis, Int. J. Quant. Chem. **S2,** 35 (1968).

[23] D. E. Ellis and G. S. Painter, Phys. Rev. **2,** 7887 (1970).
[24] D. M. Drost and J. L. Fry, Phys. Rev. **B5,** 684 (1972).
[25] J. Callaway and J. L. Fry, in *Computational Methods in Band Theory,* P. M. Marcus, J. F. Janak, and A. R. Williams, Eds. (Plenum Press, New York, 1971), p. 512.
[26] E. W. Stout and P. Politzer, Theor. Chim. Acta **12,** 379 (1968); B. J. Duke, Theor. Chim. Acta **9,** 760 (1968).
[27] R. N. Euwema, D. J. Stukel, and T. C. Collins, in *Computational Methods in Band Theory* P. M. Marcus, J. F. Janak, and A. R. Williams, Eds. (Plenum Press, New York, 1971), p. 82.
[28] D. J. Stukel, R. N. Euwema, F. Herman, and R. L. Kortum, Phys. Rev. **179,** 740 (1969).
[29] D. J. Chadi and M. L. Cohen, Phys. Rev. **B7,** 692 (1973); **8,** 5747 (1973).
[30] S. L. Cunningham, Phys. Rev. **B10,** 4988 (1974).
[31] A. R. Lubinsky, D. E. Ellis, and G. S. Painter, Phys. Rev. **B11,** 1537 (1975).
[32] R. Keown, Phys. Rev. **150,** 568 (1966).
[33] L. Kleinman and J. C. Phillips, Phys. Rev. **116,** 880 (1959).
[34] G. S. Painter, D. E. Ellis, and R. Lubinsky, Phys. Rev. **B4,** 3610 (1971).
[35] R. S. Mulliken, J. Chem. Phys. **56,** 792 (1952).
[36] P. O. Löwdin, J. Chem. Phys. **18,** 365 (1950).
[37] (a) R. N. Euwema and R. L. Green, J. Chem. Phys. **62,** 4455 (1975); (b) R. N. Euwema, D. L. Wilhite, and G. T. Surrat, Phys. Rev. **B7,** 818 (1973).
[38] Data collected by R. J. Weiss, in *X-Ray Determination of Electron Distributions* (Wiley, New York, 1966), p. 136.
[39] M. Renninger, Acta. Cryst. **8,** 606 (1955).
[40] See, for example, F. Seitz, in *Modern Theory of Solids* (McGraw-Hill, New York, 1940), p. 61.
[41] F. Herman and S. Skillman *Atomic Structure Calculations* (Prentice Hall, Englewood Cliffs, N.J., 1962).
[42] J. C. Slater, J. Chem. Phys. **57,** 7289 (1972).
[43] P. D. De Cicco, Ph.D. Thesis, Department of Physics, M.I.T., 1951, unpublished.
[44] W. E. Rudge, Phys. Rev. **181,** 1073, 1033 (1969).

Received March 15, 1976